**Conductance of perovskite oxide thin films and interfaces**
Mubeen Dildar, I.

**Citation**
Mubeen Dildar, I. (2013, February 6). *Conductance of perovskite oxide thin films and interfaces*. *Casimir PhD Series*. Retrieved from https://hdl.handle.net/1887/20501

| | |
|---|---|
| Version: | Not Applicable (or Unknown) |
| License: | Licence agreement concerning inclusion of doctoral thesis in the Institutional Repository of the University of Leiden |
| Downloaded from: | https://hdl.handle.net/1887/20501 |

**Note:** To cite this publication please use the final published version (if applicable).

Cover Page

The handle http://hdl.handle.net/1887/20501 holds various files of this Leiden University dissertation.

**Author**: Mubeen Dildar, Ishrat
**Title**: Conductance of perovskite oxide thin films and interfaces
**Issue Date**: 2013-02-06

# 6

# Interfaces of $LaAlO_3/SrTiO_3$ made by sputter deposition

## 6.1 Introduction

We have discussed the properties of the two dimensional electron gas at the interface between the band insulators $LaAlO_3$ (LAO) and $SrTiO_3$ (STO), and the mechanisms behind its formation in chapter 2. Ohtomo & Hwang were the pioneers to introduce such conducting interfaces in 2004 [1], which they ascribed to an intrinsic doping mechanism driven by the broken symmetry at the interface. In LAO, alternating layers of LaO and $AlO_2$ are positively (negatively) charged, while the SrO and $TiO_2$ layers in $SrTiO_3$ are neutral. This mechanism of electronic reconstruction is important, as can be seen in the fact that a minimum LAO layer thickness of 4 unit cells is needed to create the conducting interface, and that the STO surface needs to be terminated with a $TiO_2$ layer, furnishing Ti 3d orbitals at the interface. It is not the only possible mechanism however, and surprisingly, there is still considerable debate about the relative importance of the different factors which conspire to produce a conducting interface [2].

In particular important is the question of oxygen deficiencies, as can be appreciated from the fact that the properties of the LAO/STO interface crucially depend on the pressure of the background oxygen, at least when grown by Pulsed Laser Deposition (PLD) [3–5]. In general, the conductivity decreases with increasing oxygen pressure, and it was recently reported that at a pressure of $5\times10^{-2}$ mbar, which is close to the upper limit for the PLD process, the interface became insulating [6]. On the other hand, Cancellieri et al showed that interfaces grown at $10^{-2}$ mbar could be made superconducting when subjected to a postanneal treatment [7]. Clearly, the mobility of oxygen through the different layers during and after growth is a relevant parameter. Also cation intermixing at the interface was shown to play a role [8–10], and in a recent study on samples grown by Molecular Beam Epitaxy it was found that the La to Al ratio of the LAO layer needs to be

smaller than 1 in order to activate the interface conductance [11]. This issue has not yet been addressed at all in PLD grown interfaces.

The overwhelming majority of studies of the LAO/STO interface has been performed on PLD-grown samples. Given the promise for applications in oxide electronics [2, 12], the question is valid whether interfaces with similar (conducting) properties can be prepared by sputter deposition, a question which to our knowledge has not yet been addressed.

Sputter deposition of oxides takes place at high oxygen pressures (typically 1 mbar), which again raises the issue of the behavior of oxygen atoms and vacancies. In this chapter, we report such experiments. The interfaces between $LaAlO_3$ and the $TiO_2$-terminated surface of $SrTiO_3$ substrate are grown by RF sputtering in an oxygen atmosphere as described in section 6.2. In our deposition system, the optimized growth pressure and growth temperature for the best film and interface quality are 0.8 mbar and 920°C. The surface of the LAO films is characterized by AFM and XPS, thickness and lattice constants of films are measured using x-rays, details are given in section 6.2. As shown in section 6.3, we do not observe conductance, nor can we render the interface conducting after postannealing. In section 6.4, interfaces of films are studied by TEM and EELS. Moreover, in TEM/EDX measurements, we find that the La/Al ratio in the $LaAlO_3$ film is 1.07. It appears that this ratio is connected to the high pressure, and is also material in allowing oxygen diffusion to and from the interface. The results are compared with the low pressure PLD grown samples and discussed in detail in section 6.5. It is found that these films, which do yield conducting interfaces, are Al-enriched.

In section 6.6, the magnetic properties of sputtered grown interfaces are discussed. It is found that sputtered grown non-conducting interfaces are also non-magnetic.

## 6.2 Sputter grown LAO/STO interfaces

Crystal growth being a non-equilibrium kinetic process is generally difficult to control in any type of deposition, since it depends on a large number of parameters such as temperature, process gas pressure, mismatch between substrate and film lattice parameters, energy of the deposited particles, surface mobility etc. In the case of growing complex oxides with reactive RF sputtering, the reaction between gas and emitted target particles is assisted by substrate heating to ensure the formation of the desired film structure and stoichiometry.

Basically, to grow stoichiometric thin films of $LaAlO_3$, a stoichiometric $LaAlO_3$ target (La=1, Al =1) is chosen. All LAO films are grown on STO substrates, singly terminated by a $TiO_2$ surface. The singly terminated surfaces were commercially prepared by the company TSST B.V, Enschede, the Netherlands. For a given forward power and target-to-sample distance, two critical parameters which control the growth in sputtering are the deposition temperature $T_{dp}$ and the pressure $P_{dp}$. We determined a window for ($T_{dp}$, $P_{dp}$) for smooth and epitaxial growth of $LaAlO_3$ on $SrTiO_3$ which proved to be rather narrow. The determination is mainly based on

| $P_{dp}$ (mbar) | $T_{dp}(^oC)$ | Rough.(nm) | $c_o$ (Å) | $d_{LAO}$ | $t_{dp}$ (Min.) | Sample ID |
|---|---|---|---|---|---|---|
| 1.2 | 800 | 1.6 | x | 5 | 120 | LA44 |
| 1.2 | 840 | 1.7 | x | 15 | 306 | LA37 |
| 1.2 | 900 | 2.1 | x | 8 | 60 | LA48 |
| 1.2 | 1034 | 0.2 | 3.786 | 13 | 120 | LA47 |
| 1.0 | 840 | 1.4 | 3.789 | 13 | 160 | LA38 |
| 0.8 | 840 | 2 | 3.789 | 13 | 120 | LA36 |
| 0.8 | 920 | 0.2 | 3.786 | 20 | 120 | LA51 |
| 0.8 | 920 | 0.4 | 3.777 | 12 | 90 | LA69 |
| 0.8 | 940 | 0.2 | 3.766 | 12 | 90 | LA72 |
| 0.6 | 940 | 0.8 | 3.799 | 14 | 100 | LA68 |
| 0.4 | 940 | 0.2 | x | 15 | 60 | LA67 |
| 0.28 | 840 | 22 | x | x | 30 | LA9 |

Table 6.1: Sputter deposition parameters of $LaAlO_3$ on $SrTiO_3$. Given are the sputter gas pressure $P_{dp}$, the substrate temperature $T_{dp}$, the roughness of the LAO film as measured by AFM, the out-of-plane lattice constant $c_o$, the LAO film thickness, growth time in $t_{dp}$ (minutes) and the identifier of each sample. The forward power used to grow these films is 30 W.

AFM surface roughness. The out-of-plane lattice constant $c_o$ was also monitored, although its significance is more complicated, since it can be influenced by the stoichiometry as will be discussed. It can be noted that the growth rate for the films grown at 1.2 mbar is quite low when compared to the films at 0.8 mbar.

Before giving some details, the main results are presented in Table 6.1, where the roughness and $c_o$ values are given for film growth in a pressure range between 1.2 mbar and 0.28 mbar, and a temperature range between 800 °C and 940 °C. Smooth and epitaxial films are grown around 920 °C-940 °C and 0.8 mbar. Growing outside this window results in rough and structurally defective films. More trends are visible in Table 6.1. At 1.2 mbar, smooth films can be grown, but that requires very high temperature. Films grown at 0.6 mbar are smooth, but they have larger lattice constants than bulk LAO, which indicates the films are not correctly strained. At 0.4 mbar, films are smooth but no peak of LAO film can be seen in diffraction experiments. The lowest growth pressure used to grow LAO films is 0.28 mbar. The surface is then very rough as we will see back sputtering impedes the growth of LAO film.

Thin films of LAO were grown in a wide thickness range from 2 nm to 51 nm although for the optimized growth parameters (920 °C and 0.8 mbar), the range is between 2.5 nm and 30 nm. After deposition, films were cooled down in vacuum. It takes about 5 hours to cool down to room temperature. Some films were cooled down in the growth pressure of 0.8 mbar, but no significant change in morphology, lattice constant, XPS elemental spectra and conductivity was observed. The distance between target and substrate was about 4 cm which gives a growth rate of 0.16 nm/min for optimized $P_{dp}$ = 0.8 mbar, $T_{dp}$ = 920°C, P = 30 W. With this

| Power (W) | Rough.(nm) | $c_o$ (Å) | $d_{LAO}$ (nm) | $R_{dp}$ (nm/min) | Sample ID |
|---|---|---|---|---|---|
| 30 | 0.1 | 3.786 | 21 | 0.16 | LA53 |
| 40 | 0.2 | 3.788 | 32 | 0.27 | LA54 |
| 50 | 0.4 | 3.773 | 35 | 0.3 | LA55 |
| 60 | 0.4 | 3.799 | 51 | 0.43 | LA56 |
| 70 | 0.2 | 3.808 | x | x | LA57 |
| 80 | 0.2 | 3.817 | x | x | LA58 |
| 90 | 0.3 | 3.813 | x | x | LA59 |

Table 6.2: Effect of forward power on LAO films grown at $T_{dp}$ = 920°C and $P_{dp}$= 0.8 mbar. Given are the forward (FW) power, the roughness of the LAO film, the out-of-plane lattice constant $c_o$, the LAO film thickness, rate of deposition $R_{dp}$ and relative identity (ID) for each sample.

pressure and temperature, decreasing target to substrate distance to 2 cm increased the growth rate but no change on quality of thin films.

We also investigated the effects of changing the forward power for growth in the window ($T_{dp}$ = 920°C and $P_{dp}$= 0.8 mbar). As can be seen in the Table 6.2, increasing forward power from 30 W first increases the roughness, while above 60 W the value of $c_o$ started to increase. Apparently, both a lower sputter gas pressure and high RF power leads to more energy being deposited during growth, and a loss of strain, e.g., epitaxy. In the next two paragraphs we give more details on the AFM and XRD results.

### 6.2.1 Surface characterization by AFM

We discussed in the previous section that the sputtering allows a small temperature and pressure window to work in. We have grown a large number of films to find out the right growth parameters. The first step is to check the quality of film using atomic force microscopy (AFM). AFM software was used for the image rendering, data smoothing, height profiles and roughness analysis using a standard area of 1$\mu$m, mostly shown for images in this section and in Table 6.1.

Figure 6.1 shows the results of some films grown at 2 mbar of oxygen at different temperatures. The growth time is 15 minutes for all. The change in temperature has a clear effect on the morphology. The film grown at 800°C shows grains and the roughness is high (1.6 nm). The film grown at 840°C has decorated steps. The film is very smooth (0.3 nm). The film grown at 870°C is rough again (1.7 nm) and shows some outgrowths along with irregular terraces.

We observe that LA3 grown at 840°C looks better in morphology than the other two films. The next step is to reduce the pressure but keep the temperature at 840°C. The resulting films with the corresponding morphological changes are shown in Figure 6.2. The film at 0.8 mbar shows nicely spaced steps while the film 0.28 mbar has larger grains forming like clusters and is very rough (35 nm). Smooth films (0.3 nm) are grown at 0.8 mbar and 920°C. Figure 6.3 shows the

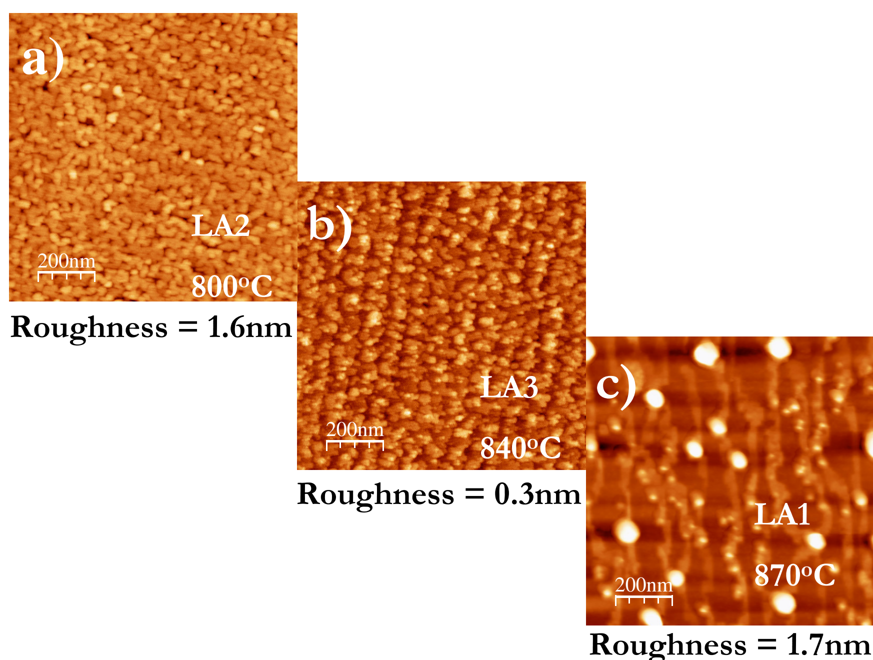


Figure 6.1: Surface morphology of LAO film grown at 2 mbar of oxygen pressure for 15 minutes. (a) LA2 grown at 800°C (b) LA3 grown at 840°C (c) LA1 grown at 870°C.

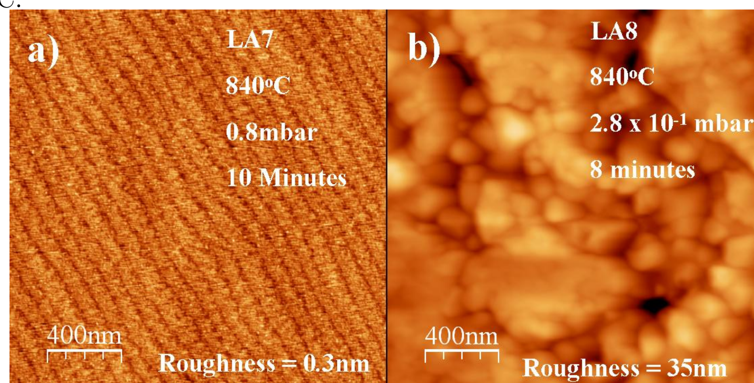


Figure 6.2: Surface morphology of LAO films grown at 840°C for approximately the same time at different growth pressures. (a) LA7 grown at 0.8 mbar of oxygen pressure (b) LA8 grown at 0.28 mbar of oxygen pressure.

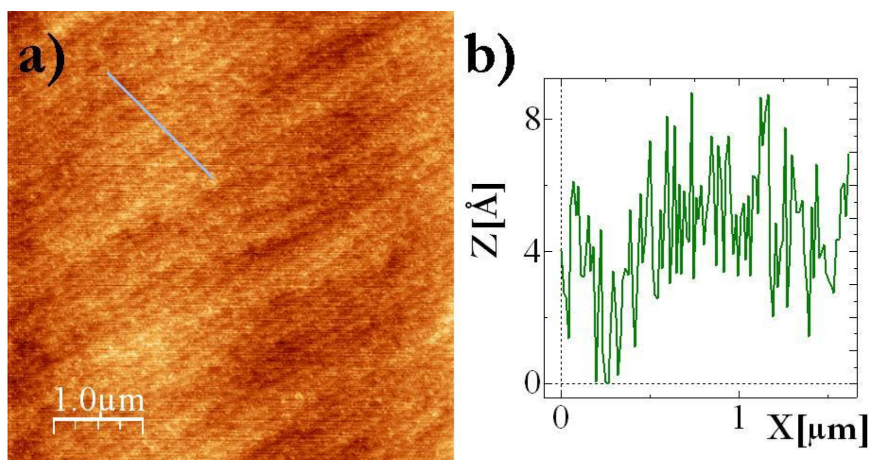


Figure 6.3: Surface morphology of a 20 nm thin film of LAO grown at 920°C, 0.8 mbar of oxygen pressure (a) topography (b) height profile of (a).

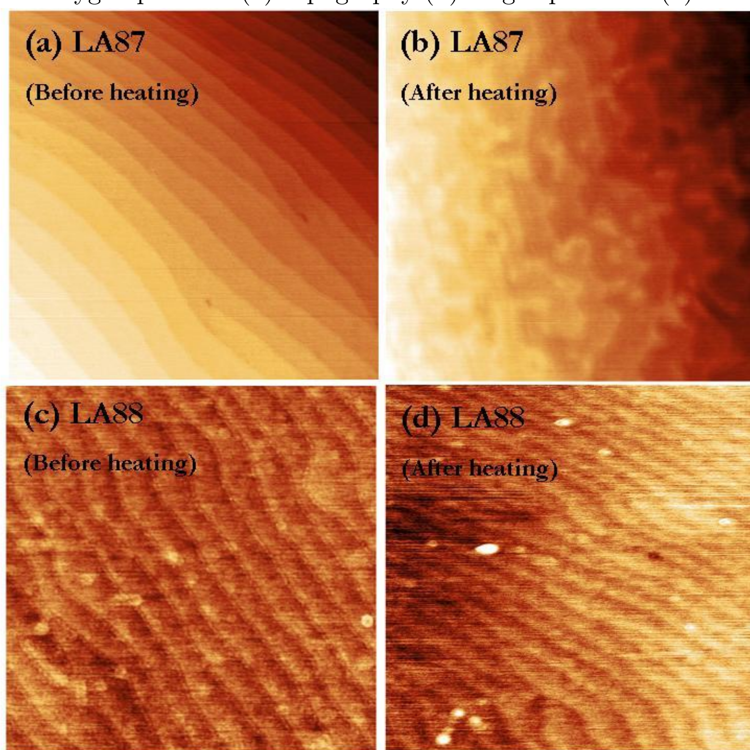


Figure 6.4: Surface morphology of a $SrTiO_3$-$TiO_2$ terminated surface before and after passing thorough the deposition steps without growing film (a & c). After heating to 920 °C the substrate is (b) cooled down in vacuum (LA87), (d) cooled down in 0.8 mbar of oxygen (LA88).

surface morphology of a 20 nm film (LA51). The corresponding profile (figure 6.3b) indicates roughness of 0.2 nm, probably connected to standard unit cell steps of 0.4 nm.

To see the effects of the high temperature growth and the cooling procedure on the $TiO_2$-terminated surface of the STO substrate, some substrates were passed through all deposition steps without depositing a $LaAlO_3$ film. The surface morphology of the samples before and after heating is shown in Figure 6.4. The samples were heated up to 920°C at 0.8 mbar of oxygen pressure and remained at that temperature for 10 minutes and then cooled down to room temperature in two different ways. The sample shown in Figure 6.4a was cooled down in vacuum and the sample shown in figure 6.4c was cooled down in oxygen pressure of 0.8 mbar. There is no appreciable change in morphology measured by AFM before and after heating, although the terrace structure in the oxygen-cooled down sample is somewhat better preserved. Since this comes closer to the growth conditions (the vacuum can cause additional oxygen loss from the substrate), we conclude that the starting surface for growth is unchanged by the high temperature.

### 6.2.2 Characterization by XPS

In the early stage of finding the growth window, x-ray photoelectron spectroscopy was used. Figure 6.5 shows spectra of two LAO films grown at 2 mbar and 0.28 mbar of pressure at a temperature of 840°C. A wide range of binding energies is measured to obtain information about the element present at the surface. Figure 6.5a shows peaks of La and Al and also small peaks of Sr and Ti while in Figure 6.5b, almost only Sr is visible. This strongly suggests that at 0.28 mbar, back-sputtering is strong enough to prevent film deposition.

### 6.2.3 Thickness measurement of $LaAlO_3$ films by XRR

The measurement in this subsection and the next one was performed by Dr. Harkema at the University of Twente, the Netherlands.

Figure 6.6 shows an XRR measurement of a 20 nm thin film of LAO on STO grown at 0.8 mbar and 920°C (LA51). Thickness fringes are clearly visible which indicate a uniform film thickness. The measured data could be well fitted with a model consisting of a 20.33(9) nm thick LAO film of uniform density using Bruker XRD software. The film/air interface has a roughness of 0.21(3) nm; the roughness of the STO/LAO interface was found to be 0.6(2) nm. Both values for the roughness are indications for epitaxial interfaces, consistent with the AFM data shown in Figure 6.3. The roughness of the interface hints at the possibility of intermixing, which is often found in this system. We shall come back to the intermixing issue in section 6.4. The constant density for within the layer indicates homogeneous films over the whole thickness range as shown in Figure 6.6b.

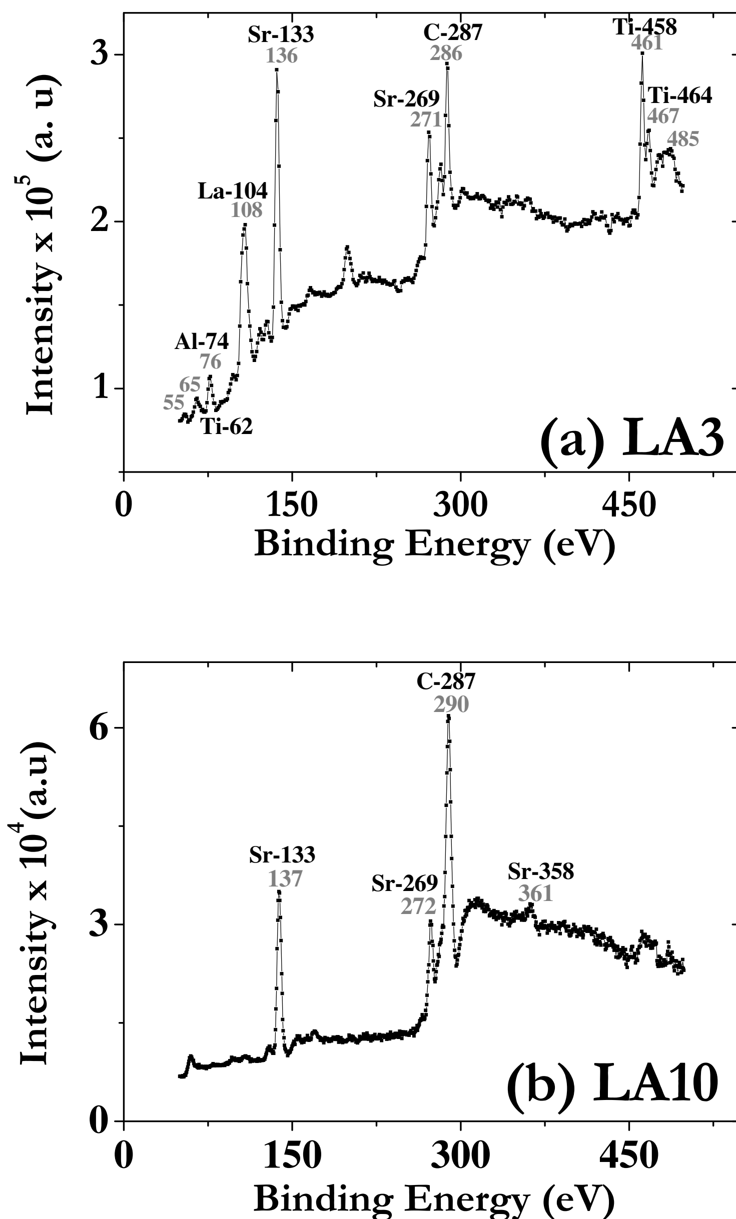


Figure 6.5: An X-ray photoelectron spectroscopy of two LAO films on STO. (Left) grown at 2 mbar and 840 °C, shows the peaks of La and Al with strong peak of Sr and small peaks of Ti, (Right) grown at 0.28 mbar and 840 °C shows diffusion of Sr at the surface of LAO film.

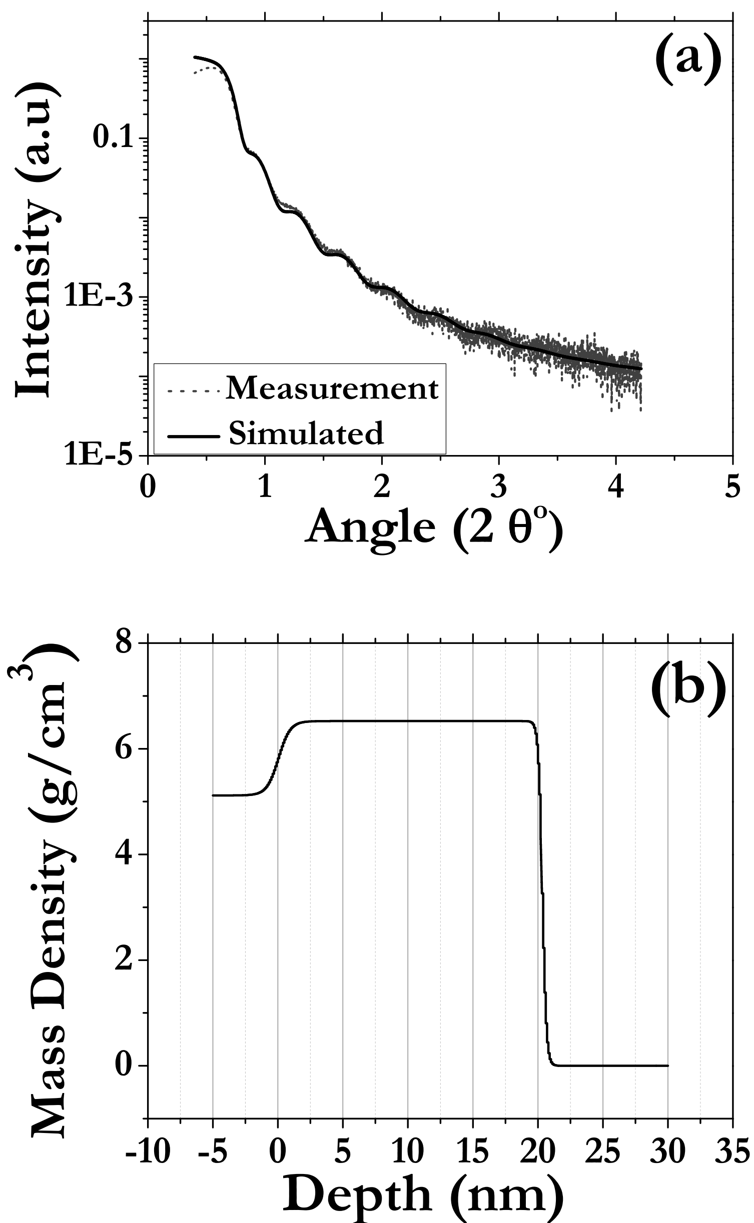


Figure 6.6: (a) An X-ray reflectivity curve for a 20 nm thick film (LA51). The period of oscillation determines the thickness of film, the drawn black line is a simulation. (b) A mass density analysis of the same 20 nm thick film to check the homogeneity of film in the whole depth range, The interface is at 0 depth.

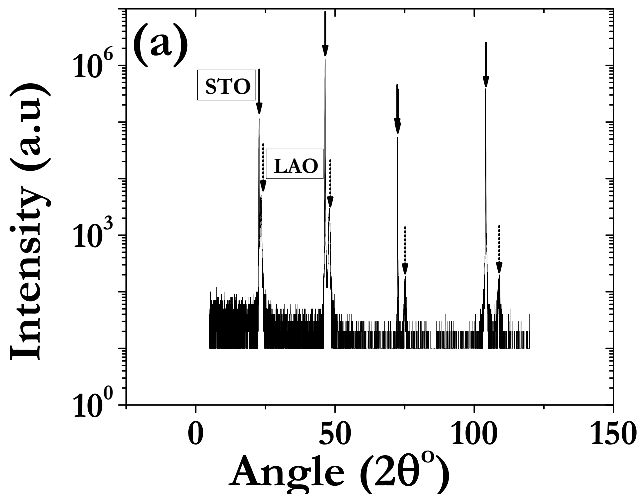


Figure 6.7: The diffraction data of a 20 nm thick film (LA51) showing 00l reflections of substrate and film. The solid arrows are for STO substrate and dotted arrows are for the LAO thin film.

### 6.2.4 Structure of $LaAlO_3$ thin films by XRD

The out-of-plane lattice constant $c_o$ of the LAO films was measured by XRD. As an example showing the reflection the $\theta/2\theta$ scans of a 20 nm thick film of LAO is given Figure 6.7a.

Figure 6.8 shows three representative films with thicknesses 12 nm, 20 nm (LA51) and 51 nm. The values of $c_o$ are given in Table 6.1. Comparison with the bulk lattice constant of LAO ($a_o$ = 3.789 Å) shows that the 12 nm film is fully strained, and the 51 nm film has a lattice parameter even sightly larger than the bulk value. The 51 nm film was grown at 0.8 mbar, 920 °C, 60 W, so at larger forward power than the 12 nm and 20 nm films.

## 6.3 Interface Conductance

We determined the conductance of a number of films at room temperature. To approach the buried interface made by LAO/STO, wires were bonded for a 2-point or 4-point measurement, with contacts in line using a wire bonder. The typical distance between the voltage contacts was 1 mm. The samples were measured in a physical properties measuring system (PPMS) with external current and voltage sources. Typical values of the sheet resistance were 10 MΩ and above, limited by the voltage and current sources. Four films (with thickness of 12 nm, 13 nm, 14 nm and 30 nm ) were cooled down to 10 K, but showed no variation in conductance

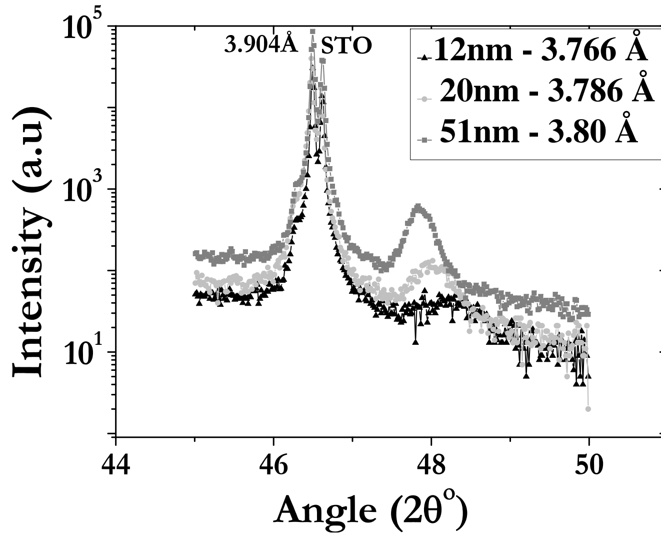


Figure 6.8: XRD data of three representatives films of LAO at angles around the [002] reflection. The [002] STO peak corresponds to a lattice parameter of 3.904 Å. The square symbols show a 51 nm thick LAO film (LA56), the circles are for a 20 nm film (LA051), the triangles are for a 12 nm film (LA72). Also given are the lattice parameters of the films as calculated from the intensity peaks.

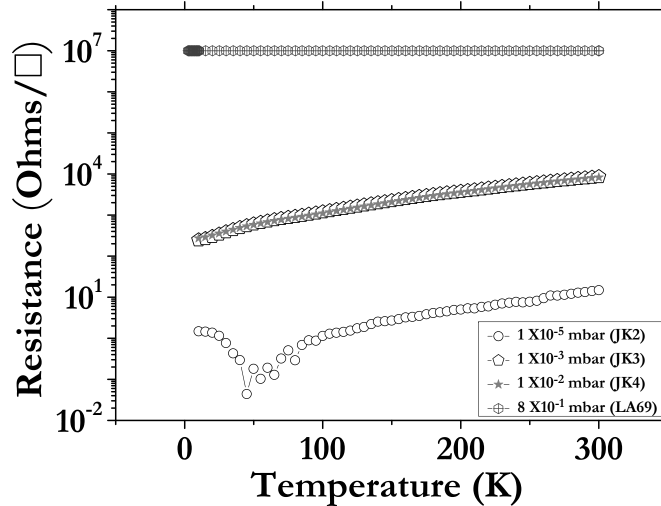


Figure 6.9: The resistance versus temperature behavior of interfaces grown by PLD at pressures of $10^{-5}$ mbar (JK2), $10^{-3}$ mbar (JK3), $10^{-2}$ mbar (JK4) respectively for a 5 nm $LaAlO_3$ film and by sputtering at 0.8 mbar of pressure for a 12 nm thin film of LAO (LA69).

(Figure 6.9). Post-annealing did not change this behavior. The details of post annealing are given in the next paragraph. To test the measurement setup, we obtained a series of films from the University of Twente (courtesy Dr. J. Kleibeuker). We measured the conductivity of PLD grown interfaces of $LaAlO_3/SrTiO_3$ grown at different pressures using Van der Pauw geometry. The conductivity of these samples (denoted by JK2, JK3, JK4) is shown in Figure 6.9.

**Post-annealing**

Insulating interfaces grown by PLD at $10^{-2}$ mbar can be made conductive by post annealing [7]. Therefore, rather than using the standard procedure of cooling, some samples were cooled down to 580°C. The oxygen pressure was then raised to 0.2 bar while the sample cooled further to 530°C in about 15 minutes. These conditions were maintained for 1 hour before cooling down to room temperature. Such samples still did not show conductance.

## 6.4 The LAO/STO Interface

To probe the interface between LAO/STO, transmission electron microscopy (HR-TEM), energy dispersive x-ray (TEM/EDX) and electron energy loss spectroscopy (EELS) were used in a collaboration with the group of Prof. H. Zandbergen at Delft University of Technology.

### 6.4.1 Quality of interface

The insulating interfaces made by sputtering need to be investigated in detail in particular to find out whether the quality is sufficient to make conductance over the macroscopic lengths possible. For this purpose, we used transmission electron microscopy which uses a high energy electron beam transmitted through a very thin sample to image and analyze the microstructure with atomic-scale resolution.

As we discussed earlier, sputtering allows a small window for crystalline films. Here we show interfaces of a few samples grown at different temperature and pressure. Figure 6.10 shows the TEM image of two films of LAO on STO, LA37 and LA47 which were grown at $P_{dp}$ = 1.2 mbar and $T_{dp}$ = 840°C and 1034°C respectively (see Table 6.1). Small and discontinuous patches can be seen for LA37 shown in Figure 6.10a. Figure 6.10b (LA47) looks more smooth but there are small etch pits. In these cases, it cannot be ruled out that the insulating behavior of films may be because of these discontinuities.

Figure 6.11 shows two more interfaces measured by TEM. Both films are on larger area of interface 10 nm and both show small discontinuities. Both films LA46 (1.2 mbar, 900°C, 40 W) and LA50 (1.2 mbar, 900°C, 30 W) show that the interface is rough and not continuous. There are small etch pits of around 10 nm high. Another two images of LAO thin films shown in Figure 6.12 also shows discontinuities and etch pits.

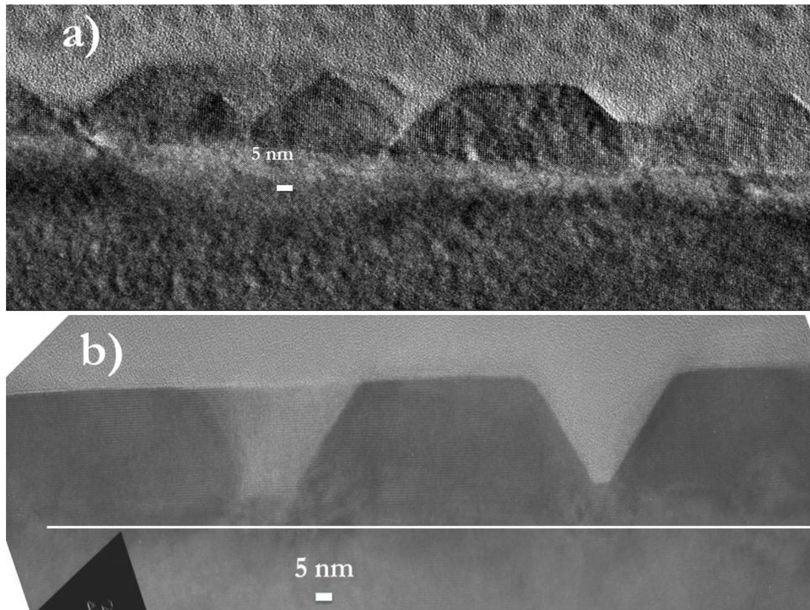


Figure 6.10: TEM analysis of two films of LAO/STO (a) LA37 (840°C, 1.2 mbar) (b) LA47 (1034°C, 1.2 mbar).

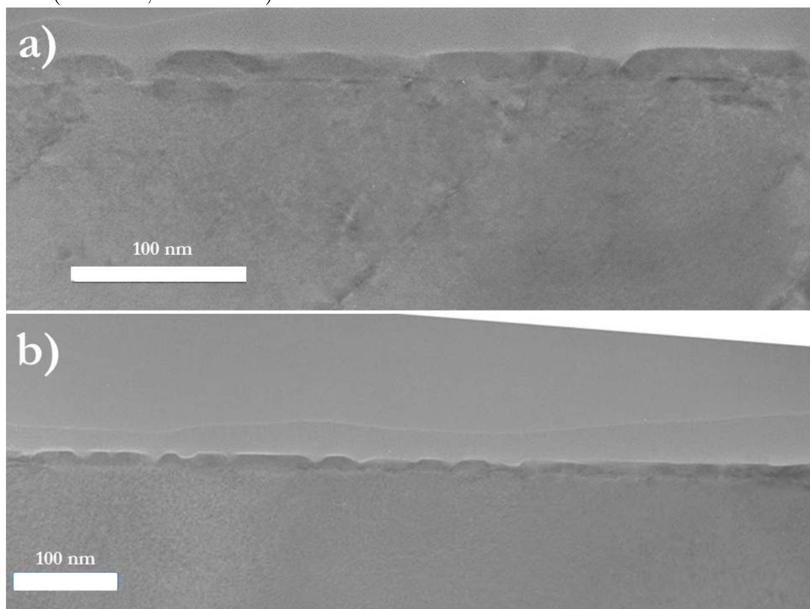


Figure 6.11: TEM analysis of two films of LAO/STO (a) LA46 (900°C, 1.2 mbar, 40 W) (b) LA50 (840°C, 1.2 mbar, 40 W).

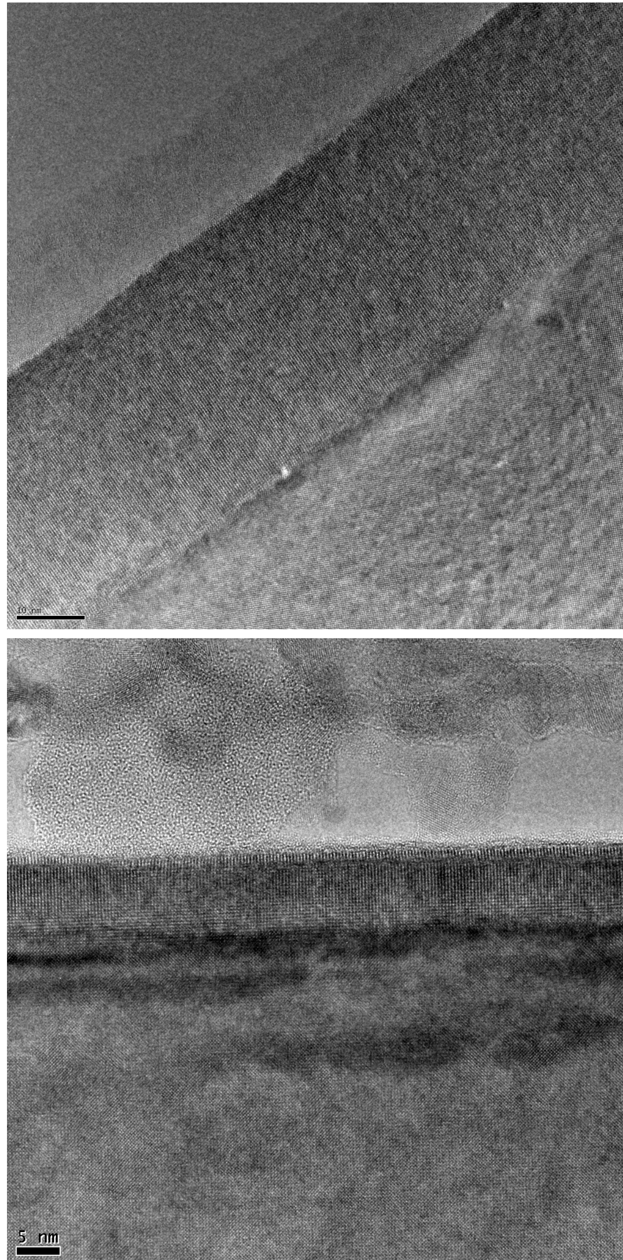


Figure 6.12: (Top) High resolution TEM picture of the LAO/STO interface for film LA55 (920°C, 0.8 mbar, 50 W). (Bottom) LA65 (940°C, 0.6 mbar, 30 W)

Figure 6.13a shows a TEM micrograph of an atomically sharp LAO/STO interface, made on film LA51. The diffractogram (figure 6.13b) shows a small splitting in the higher order diffraction spots, which point to a small misalignment between the out-of-plane crystallographic axes of LAO and STO. Similar observations were made on PLD-grown interfaces [10].

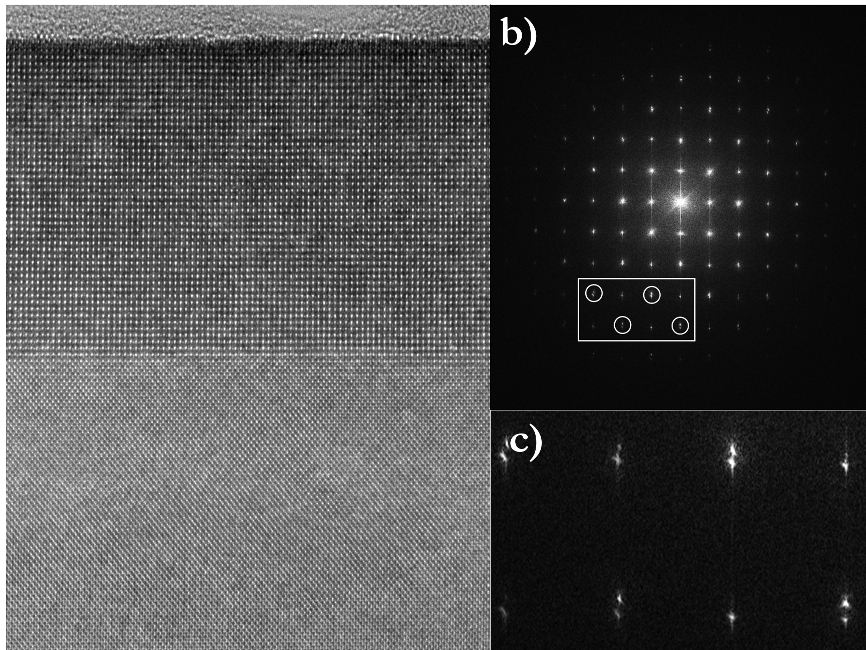


Figure 6.13: (a) High resolution TEM picture of the LAO/STO interface for film LA51.(b) Diffraction pattern. (c) Enlarged part of the region of the marked spots, showing a slight splitting which indicates some misalignment between film and substrate.

### sharpness of interface

The sharpness and the amount of interface cationic mixing was investigated in the following way. Starting with the micrograph of Figure 6.14a, the original picture was subtracted from the same picture but shifted over half a unit cell along the [110]-direction. Next, the intensity variation was derived for cross-sectional lines along a direction perpendicular to the interface. Two such lines are shown in Figure 6.14a (top), with the corresponding intensity variation in Figure 6.14b (bottom). On the LAO side of the interface, intensity still remains on the atomic positions, because of the difference in scattering factors for La and Al. On the STO

side of the interface, the Sr and Ti signals are very similar, and the subtraction brings the signal to close to zero. In this way, the crossover in the interface region gives a good estimate for the amount of intermixing, which can be seen to be of the order of two to three unit cells.

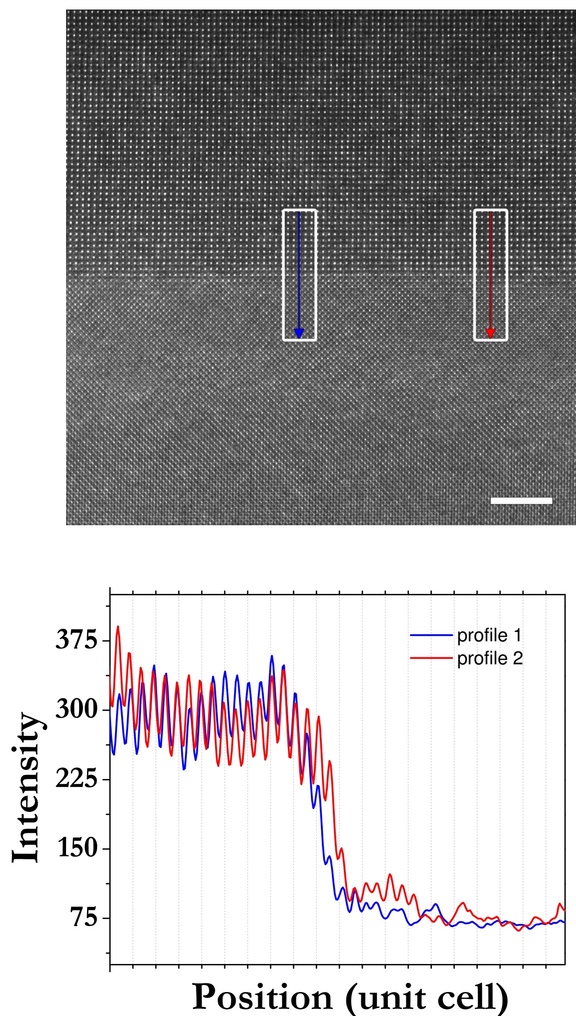


Figure 6.14: (Top) High resolution TEM picture of the LAO/STO interface for film LA51. (Bottom) Intensity variation along the two lines shown in the left figure, derived by subtracting the image from a copy of itself which was shifted by half a unit cell along the [110]-direction (see text). Note that profile 1 (blue) is shifted over one unit cell with respect to profile 2 (red).

### 6.4.2 Stoichiometry of LAO film

The elemental ratio for each element was measured by energy dispersive x-ray analysis (EDX), in particular the ratio of La to Al. This was done as follows.

A diffracted spot is chosen, shown in dark black cross in Figure 6.15a. The beam is scanned through film/interface/substratre with reference to the dark black cross. The drift is checked continuously with respect to the diffracted spectrum. A single crystal of $LaAlO_3$ was used as a reference. The measurement done on it is shown in Figure 6.15. The ratio of La/Al for single crystal LAO is found to be 0.97. The

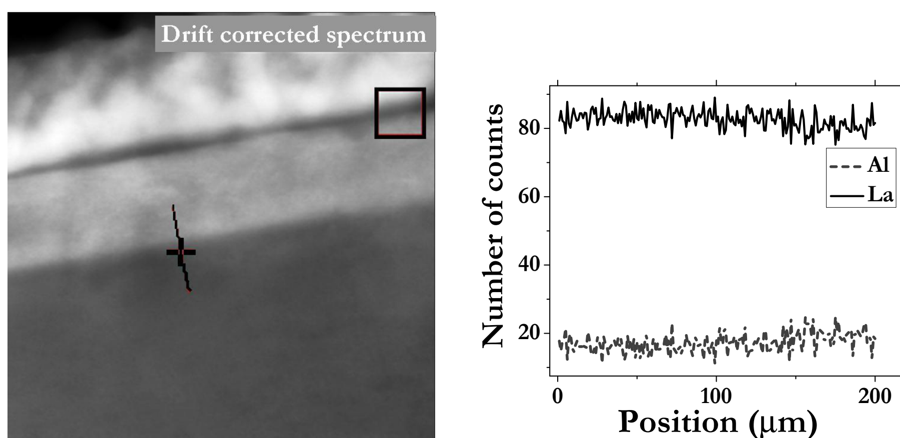


Figure 6.15: (Left) A drift corrected spectrum for precise measurement of TEM/EDX. (Right) Elemental profile of single crystal of LAO. The ratio La to Al is 0.97.

elemental variation across the LAO/STO interface was probed with EDX (beam diameter 0.2 nm) and is given in Figure 6.16. The signals are strong and stable beyond the interface region and allow to determine the elemental composition. EDX line scans were made across the LAO/STO interface, providing the atomic composition profiles as shown in Figure 6.16. The La/Al ratio of the film was obtained by averaging over 92 data points from Region 1 and calibrated by using the averaged value obtained from a $LaAlO_3$ crystal. For an accurate calibration, the EDX experimental conditions for the crystal and the film were deliberately set up in the same way, including the cross-section sample preparation, the orientation of the sample in the holder and the TEM mode settings. In this way, the La:Al ratio of the film was found to be 7 percent higher than that of the crystal. Supposing the ratio there to be 1, the La/Al ratio in the film is therefore 1.07(2).

### 6.4.3 Intermixing effects

To see intermixing effects at the interface, electron energy-loss spectroscopy (EELS) is used. EELS is a localized technique attached that measures the change in kinetic

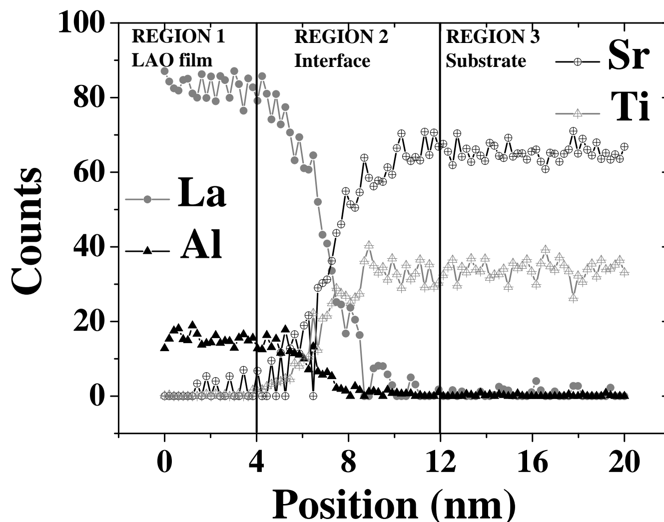


Figure 6.16: STEM/EDX elemental profile of the LAO/STO sandwich across the interface. The elemental ratios La/Al and Sr/Ti were determined in regions 1 and 3, respectively.

energy of electrons after they have interacted with a specimen. When carried out in a transmission electron microscope (TEM), EELS is capable of giving structural and chemical information about a solid down to the atomic level.

Figure 6.17 shows the EELS measurement performed on a 20 nm (LA51) thick film of LAO on STO. The TEM analysis of same film is shown in Figure 6.13. The number of counts corresponding to elements La and Ti are collected across the interface. It can be seen that La diffuses on the side of substrate while Ti diffuses on side of film which indicates that some unsharpness is found in both the change in Ti and La signal. The interface region is enlarged in part (b) of the figure. The width of the interface is 2 nm, comparable to the width in PLD grown interfaces.

### 6.4.4 Attempts to fabricate conducting interfaces

We have used oxygen as a reactive gas in RF sputtering to grow LAO films and LAO/STO interfaces which are found to be insulating. The high oxygen pressure possibly prevents the formation of oxygen defects and can compensate the deficiency of oxygen without need for pre/post annealing steps. It should be kept in mind that in PLD grown conducting interfaces, crystallinity is not an essential requirement. Amorphous films of LAO at $10^{-3}$ mbar can also make the interface conducting [24]. With this idea, we varied the growth parameters beyond the optimized growth window ($T_{dp}$ = 920°C and $P_{dp}$= 0.8 mbar). We changed the oxygen

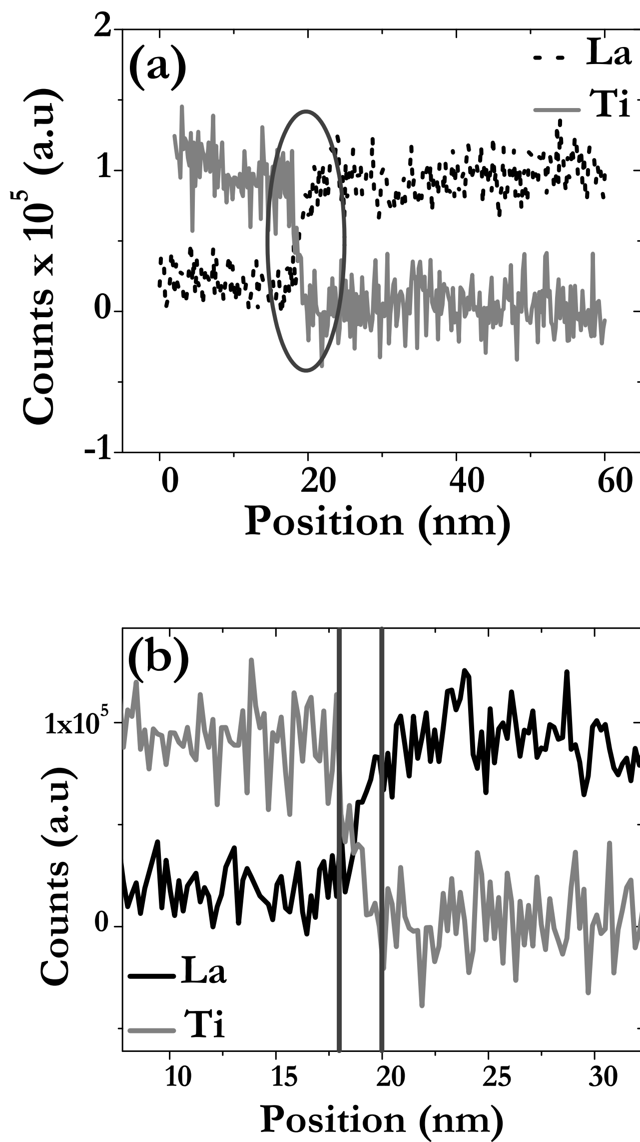


Figure 6.17: (a) EELS spectra showing the number of counts of intermixed La and Ti across the interface (b) the enlarged part at the interface showing the width of interface about 2 Å.

flow, introduced argon gas and even a mixture of argon and oxygen (50,50) but

interfaces were not conducting. Also reducing the pressure below the optimized pressure (Table 6.1) can produce amorphous films but the interface still remains non-conducting.

We also used a non-stoichiometric $LaAlO_3$ target (La=0.94, Al=1.06) to enhance the elemental contribution of Al in the grown films. There is no appreciable change in morphology, surface roughness by AFM, or lattice constant of these films. Their stoichiometry measured by TEM/EDX gives the ratio La/Al = 1.06 (LA78). So, it is not easily possible to enhance Al in growing films at high pressure oxygen environment, even with a defective target. We finally tried to put extra Al on the La-defective target in the form of pieces of Sapphire ($Al_2O_3$) to grow thin films of LAO for Al-enrichment. Clear changes can be seen in morphology but no change in the insulating state. Putting more Al resulted in roughening the surface and changing/increasing the lattice constant but conduction was not induced.

## 6.5 Discussion

The LAO films are grown at high oxygen pressure of 0.8 mbar and the interfaces are found to be insulating. The surface of the films is smooth, the structure is crystalline and the interfaces are sharp. The techniques which are used to characterize them confirm that sputtered grown interfaces are of high quality and can be compared to PLD or MBE grown interfaces. The picture from the data is then as follows.

**Electronic reconstruction**
Apparently, the sputter grown interfaces are not electrically reconstructed as in PLD. This leads us to argue that intrinsic electronic reconstruction is not the dominant mechanism. The presence of polar LAO and non-polar STO but the absence of conductance indicates a missing factor which either activates or initiates the interfacial conductance. Intermixing is not the cause since it is always there, either in PLD or sputtering . So, the polar discontinuity and intermixing do not seem to be the only or main factors determining the conductance.

**Oxygen pressure**
The sputtered interfaces grown at the high oxygen pressure of ~1 mbar closely resemble the high pressure PLD grown interfaces reported on by Kalabukhov [8] which are also insulating. This strongly hints at the important role of oxygen vacancies in conducting interfaces grown by PLD. Both in high-pressure PLD and in high-pressure sputtering, the amount of oxygen vacancies produced in the growth process becomes too low to generate a doped interface. This may not be simply due to the high gas pressure, which might be thought to quench vacancy production by highly energetic particles in the PLD- or sputter-plasma. Here, it should be remarked that the reduction of STO is difficult to rule out [6, 19]. If PLD growth parameters (750°C - 850°C, $10^{-5}$ to $10^{-3}$ mbar) can reduce STO even 10 nm or more (the interface is of the order of 2 nm), it can be enough to facilitate conduc-

tion at the interface. So, defects associated with the $SrTiO_3$ may be responsible for a conducting interface. In sputter grown films the high pressure of the background oxygen appears not to reduce the STO.

**Growth temperature**

The temperature of sputtered grown films is 920°C, which is higher than PLD grown films (typical temperature range 750°C - 850 °C). We would argue that the higher growth temperature is not the reason for the lack of conductance. There are two main reasons for that. First, STO substrates are annealed at high temperature (1300 °C) to produce the singly terminated $TiO_2$ surface. Second, $TiO_2$ terminated STO substrates were passed through the deposition steps without LAO films, cooled down in vacuum and growth pressure of 0.8 mbar and were checked by atomic force microscopy (AFM). This showed that no appreciable change in termination had occurred. Note that in PLD grown films the sheet resistance goes down with thickness [25], but that at 10 nm, there is still an appreciable dependence of the conductance , which we do not find in the sputter-grown films.

**Strain, external electric field and post-annealing**

The non-conductance of interfaces grown by sputtering does not change with strain. We have grown films on a large scale variation (Table 6.1) with respect to the out of plane lattice parameters of the LAO films but none of the samples has shown conductance. We also applied an electric field to these non-conducting interfaces to tune the interfacial conductance but found no change in insulating behavior. Post-annealing (the detailed process is discussed in section 6.3) also did not change the status of interfaces grown by sputtering. The results of Cancellieri *et al* [7] who converted initially non-conducing interfaces to conducting ones by post-annealing, strongly suggest that their LAO film allows the oxygen content of their interface to be varied. These three factors strain [26], electric field) [17] (in the underlaying STO) and post-annealing [7] were able to induce or change the conductance of the interface grown by PLD but remained inactive for insulating interfaces grown by sputtering.

**Stoichiometry**

Next we come to the issue of stoichiometry, which until now has received relatively little attention. We start from the report mentioned in section 2.4.4, where it was demonstrated that the interface between STO and MBE-grown LAO was only conducting as long as the La/Al ratio was below 0.97. By inference, we assume for the moment that this means that the LAO film of a conducting PLD-grown STO/LAO interface also has a La/Al ratio below 0.97. As was shown in section 6.4.2, the sputtered samples have a ratio above 1, and this may have important consequences. For instance it was shown by Schneider *et al* that oxygen is drawn out of the STO substrate in the case of LAO films grown at low oxygen pressure ($1.5 \times 10^{-5}$ mbar), which were probably Al rich [14]. Such a mechanism to create oxygen defects may not be present in La-rich films, as was surmised by Chambers [15]. This is also of relevance for the post-annealed experiments of Cancellieri

| $P_{dp}$ (mbar) | Deposition process | La/Al ratio | Sample ID |
|---|---|---|---|
| $8\times10^{-1}$ | Sputtering | 1.07 | LA51 |
| $8\times10^{-1}$ | Sputtering | 1.066 | LA78 |
| $1\times10^{-5}$ | PLD | 0.82 | JK2 |
| $1\times10^{-3}$ | PLD | 0.856 | JK3 |
| $1\times10^{-2}$ | PLD | 0.90 | JK4 |
| $1\times10^{-1}$ | PLD | 1.03 | JK8 |

Table 6.3: Summary of EDX measurement for sputter-grown and PLD grown samples. $P_{dp}$ is the deposition pressure, corresponding La to Al ratio in PLD and sputtering and relative samples are also given.

*et al*, since their PLD-grown LAO is probably La deficient, allowing removal of oxygen [7].

In our case, the stoichiometry of sputter grown samples from a stoichiometric target measured by EDX gives La-rich films with a La to Al ratio of 1.07. The same ratio is obtained for a defective target of $LaAlO_3$ (La = 0.94, Al = 1.06). It shows that high pressure sputtering yields Al deficient films. This may not be strange as in sputtering lighter elements (here Al) can scatter more than heavier element (La). A recent study by Qiao *et al* gives an important correlation between between La to Al ratio and lattice constants of LAO films on STO using PLD [13], which is shown in Figure 6.19. They find that the out-of-plane lattice constant increases by increasing the La/Al ratio but the in-plane lattice constant does not change and remains at 3.905 Å. When the La/Al ratio is 1.22, the in-plane lattice constant decreases and LAO films are no more tetragonal. A typical value of $c_o$ = 3.78 Å for our thin strained films (Table 6.1) would correspond to a La/Al ratio of 1.10, in very good agreement with the value we find from EDX. The in-plane lattice constants of some of LAO films were measured using RSM plots in Twente University by Dr. S. Harkema. These preliminary measurements show that these films which were grown on optimized growth parameters (920°C, 0.8 mbar), have an in-plane lattice constant of 3.905 Å , and are therefore epitaxial and strained. It is interesting to note, however, that the 51 nm sample prepared with 60 W forward power (LA56) has a larger $c_o$ than bulk. This might be possible if the La/Al ratio has increased further.

With respect to the consequences of ratio's La/Al larger or smaller than 1, this was investigated theoretically by Hellberg, using first-principle DFT calculations [16]. He concluded that in La-rich films, La does not substitute for Al but instead, Al vacancies are formed . These vacancies can migrate to the interface and screen the polar discontinuity, so that the metallic interface does not form.

**Stoichiometry of PLD grown samples**

A valid question which can be raised at this point is about the stoichiometry of conducting interfaces/films grown by pulsed laser deposition. We discussed in section 6.3 and 6.4 that films grown by sputtering and interfaces are of high quality.

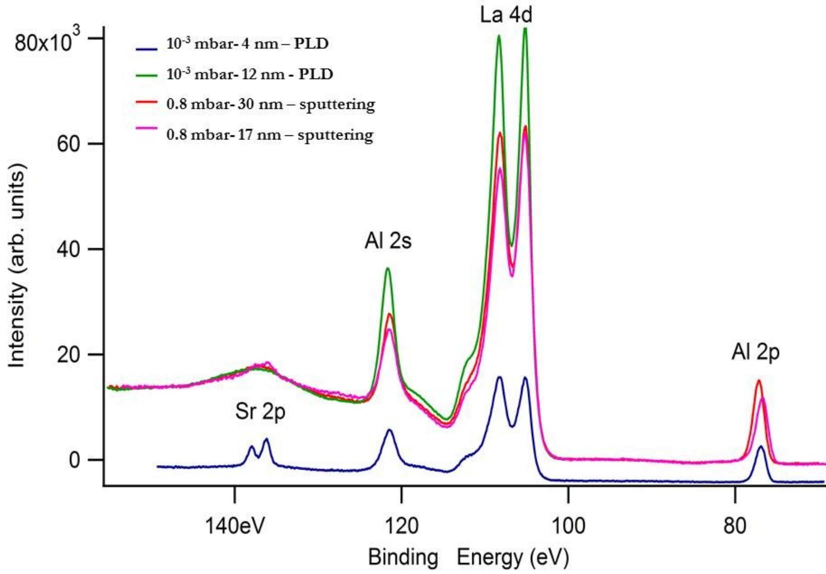


Figure 6.18: XPS spectra of PLD films grown at $10^{-3}$ mbar and sputter grown films at (0.8 mbar, 920°C - 940°C). The films shown in red line is cooled down in oxygen pressure of 0.8 mbar and in pink is cooled down in vacuum.

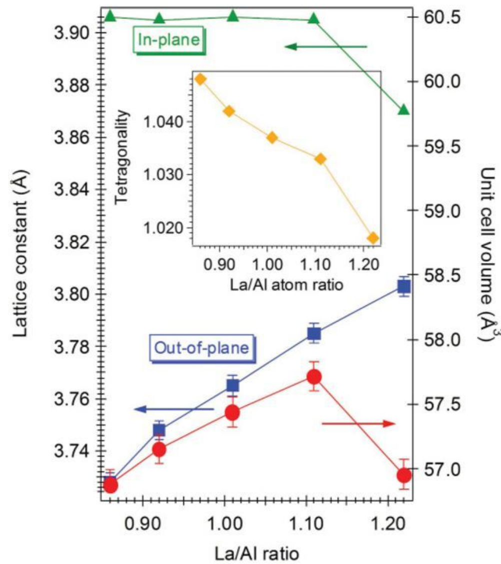


Figure 6.19: Dependence of lattice parameter and unit cell volume on La to Al atomic ratio from XRD data in PLD grown samples, the inset shows tetragonality of LAO films. The figure is taken from Ref. [13].

In Figure 6.18, we give XPS measurement of films grown by two types of deposition. The PLD samples were grown by Dr. J. Kleibeuker at Twente University, the Netherlands and she performed the XPS measurements. We can see a high intensity peak of La 4d and Al 2s, Al 2p for all samples. We also measured the ratio of La and Al in the samples grown by PLD at different growth pressures. The sample preparation for TEM/EDX measurement of all PLD grown samples is the same as discussed before in section 6.4 for sputter grown sample. The measurements show that conducting PLD samples grown at low pressure give a ratio around 0.85. The PLD grown films at the high pressure of $10^{-1}$ mbar gives the ratio of 1.03, close to sputter grown samples at 0.8 mbar (1.07). Clearly, this does not answer the question whether the La enrichment is a result of the high oxygen pressure, but it does help to understand why La-rich $LaAlO_3$ on $SrTiO_3$ does not yield conductance. Also, the La/Al ratio measured for PLD grown conducting interfaces confirm that the non-stoichiometry plays a vital role for conductance. Either Al rich films produce oxygen vacancy defects or oxygen vacancies allow the stoichiometric imbalance of the LAO films. The results of the EDX measurement are summarized in Table 6.3.

### 6.5.1 Conclusion

In conclusion, we have grown LAO/STO interfaces by sputtering in high oxygen pressure. The LAO films are smooth, strained for small thickness, and show excess of La, while the interfaces are not conducting; nor can they be rendered conducting by a post-anneal treatment. Apart from the practical implications with respect to sputtering as a technique to fabricate such conducting interfaces, the results point to the importance of the stoichiometry issue in relation to the physics.

## 6.6 Magnetic Properties of sputter grown interfaces

In the last section we showed that sputtered grown interfaces are not conducting. Here, we report the magnetic behavior of these interfaces. The magnetic properties were measured using a commercial superconducting quantum interface device (SQUID) magnetometer.

### 6.6.1 Introduction

Most of the focus in research on LAO/STO interfaces has been on their conducting properties. Recently, there has been renewed interest in the possible existence of magnetism at the interface of $LaAlO_3/SrTiO_3$. Interface magnetism was first theoretically suggested by Pentcheva and Picket *et al.* for n-type interfaces of $LaAlO_3/SrTiO_3$ (both are non-magnetic materials) who found charge imbalance at the interface to be responsible for possible ferromagnetic order [27]. At about

the same time, experimental indications for interface magnetism were first reported [20].

There are different electronic configurations possible for the interface of $LaAlO_3/SrTiO_3$ which may lead to magnetism. It was found that at the interface, most of the carriers needed to compensate for the polar discontinuity go into localized states, which strongly suggests that it is these states that give rise to the magnetization [28]. The electronic phase separation is a theoretical prediction of transferred charges at the interface of LAO/STO which occupy nearly ten interface sub-bands [29]. Indications for such an EPS state is given by Ariando *et al.* [30]. Bert *et al.* found that the magnetic regions are inhomogeneous, with patches of micrometer-scale ferromagnetic regions and a total density of magnetic moments which is approximately equal to the density of electrons implied by the polar catastrophe [31]. Li *et al.* measured the magnetic moment of LAO/STO interfaces using torque magnetometry [32]. The values they found are somewhat smaller than those measured using SQUID for samples grown under similar conditions but the order of magnitude they find is 0.4 $\mu_B$ per interface unit cell. Very recent work gives a direct relation between interface conductivity and ferromagnetism [33] where only those interfaces are found to be ferromagnetic which are also conducting above the critical thickness of four unit cells. Theoretical work of Pavlenko *et al.* showed that oxygen vacancies could locally lead to an enhanced charge density and favor a ferromagnetic state [34]. Taking into account the particular dielectric properties of STO may provide a description where electrons delocalize over a few unit cells inside the substrate [35].

It appears that interfaces of $LaAlO_3/SrTiO_3$ by pulsed laser deposition are always ferromagnetic. There can be a discussion on the amount of magnetization and it seems to vary as the conductivity of the reported interfaces vary. The growth conditions and cooling down procedure are very relevant to the different reported values. In contrast, we find that the $SrTiO_3$ substrates we use give a ferromagnetic contribution, but that the sputter-grown interfaces do not show more magnetism than what we find in the substrates. Our conclusion is that they are only slightly or even non-magnetic.

### 6.6.2 Experimental

Thin films of LAO on STO with thickness ranging from 5 nm to 20 nm were prepared using RF reactive sputtering at high oxygen pressure of 0.8 mbar at 920°C. The magnetic properties of the films were measured using a SQUID magnetometer in RSO (Reciprocating Sample Option) mode in the temperature range between 10 K to 400 K and magnetic fields up to 7 T. For reference, the magnetic susceptibility of few a STO substrates was also measured. Films were usually grown on 10 mm×10 mm×0.5 mm STO substrates. For the SQUID measurements they were cut with a tungsten wire (using Silicon Carbide powder, mesh 800 and Paraffin oil as lubricant) into pieces of 5 mm×5 mm. Some samples were also cut by a dicer with a Nickel wheel saw. Care was taken not to handle the substrates with other metallic objects but we suspect that cutting with the Ni saw might have contami-

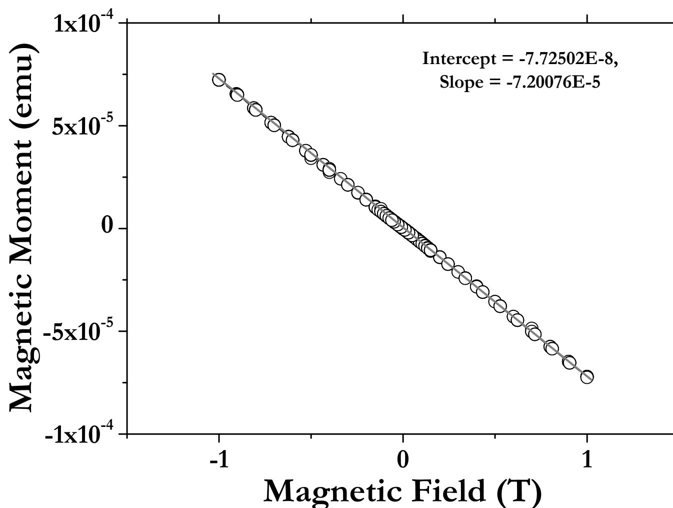


Figure 6.20: Magnetic field versus magnetic moment for an STO substrate at 300 K.

nated some STO substrates during cutting. More experiments are being performed to exclude this possibility.

The data will be given in terms of magnetic moment as measured in the SQUID from the fitted dipole signal. The cgs unit for magnetic moment is called here e.m.u, which corresponds to $10^{-3}$ $Am^2$.

### 6.6.3 Results

To quantify the origin of possible ferromagnetism in LAO/STO grown by sputtering, we used a systematic approach. A singly terminated STO substrate was measured at 5 K and 300 K and the same substrate was measured again after heating to 920 °C at 0.8 mbar of oxygen pressure without growing LAO films (defined as 0 nm LAO/STO, LA115).

First, the field dependent magnetic moment was measured as shown in Figure 6.20, for an STO substrate at 300 K. The STO substrate is diamagnetic. Using the slope of -7.2×$10^{-8}$ $Am^2/T$, sample dimensions 5 mm×5 mm×0.5 mm and a density of 5120 $kg/m^3$, we find a susceptibility of -1.4×$10^{-9}$ $kg/m^3$, in good agreement with the early experiments [36]. To check any ferromagnetism in the low field region, the diamagnetic background contribution is subtracted and the resulting moment is shown in Figure 6.21. This step was done for all measured samples and we next show only the M-H loops after diamagnetic substraction.

After background substraction, Figure 6.21 shows that the STO substrate is slightly ferromagnetic, with an $M_s$ of the order of 8×$10^{-7}$ emu at 300 K increasing

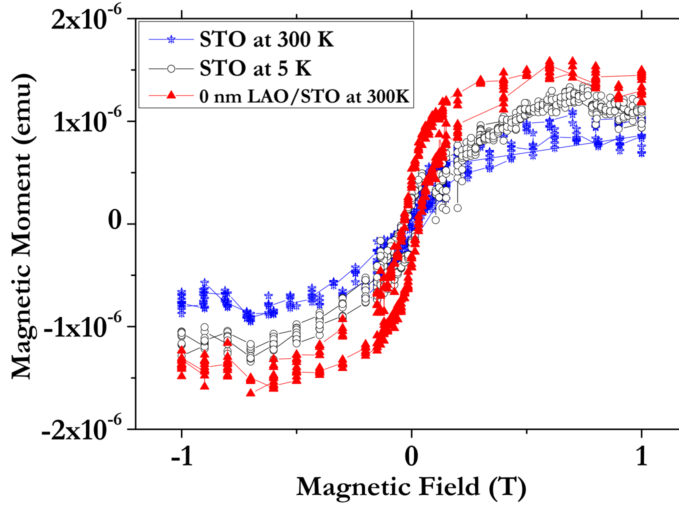


Figure 6.21: Field dependence of magnetization for STO substrates at 300 K and 5 K after subtracting diamagnetic background. A 0 nm LAO/STO (LA115) faced all deposition conditions with LAO film.

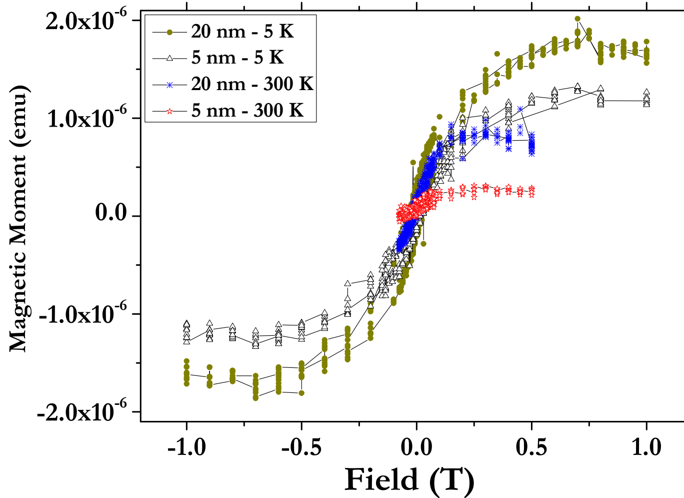


Figure 6.22: Field dependence of magnetization for a 5 nm and 20 nm films of LAO on STO at 5 K and 300 K.

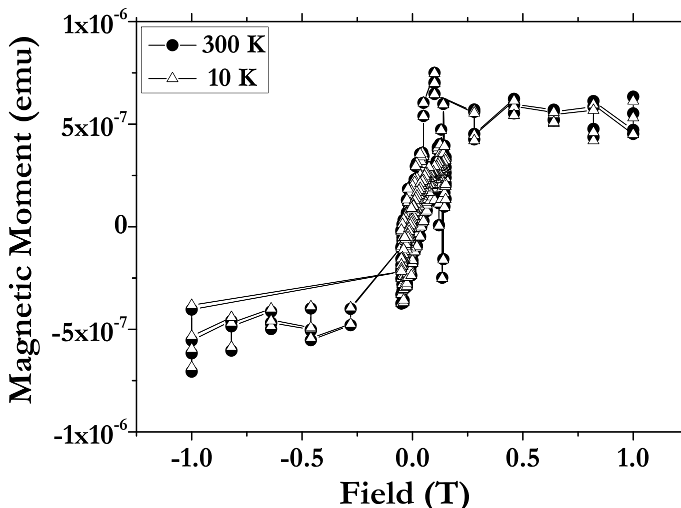


Figure 6.23: Field dependence of magnetization for a 9 nm film of LAO on STO at 10 K and 300 K.

to $10^{-6}$ at 5 K. The 0 nm LAO/STO (LA115) shows an $M_s$ of $1.5\times10^{-6}$ emu at 300 K, which means increase of a factor 2 after the annealing treatment.

Figure 6.22 shows magnetic field versus magnetic moment of 5 nm and 20 nm films of LAO on STO at 5 K and 300 K. Both samples show a small ferromagnetic loop at lower magnetic field. The difference in saturation magnetization for the 5 nm film and 20 nm film at 5 K is $7\times10^{-7}$ emu. At 300 K, the magnetic moment for both films is lower than at 5 K. The saturation magnetization for the 5 nm film and the 20 nm film is and $2.4\times10^{-7}$ emu and $8.6\times10^{-7}$ emu respectively at 300 K. Figure 6.23 shows the magnetic behavior of a 9 nm film of LAO on STO. The saturation magnetization at 10 K and 300 K is the same, $6\times10^{-7}$ emu. Figure 6.24 shows the temperature dependence of magnetization in 1 T for LAO films grown on STO substrates (singly terminated by $TiO_2$) for 9 nm, 13 nm and 17 nm thin films, a 9 nm thin film of LAO on untreated STO and on a LAO substrate. We see a gradual decrease in diamagnetism in the thin films of LAO. The highest signal is obtained for films of 9 nma and 13 nm grown on treated STO substrates. The magnetization is independent of the temperature for all film.

### 6.6.4 Discussion

Our sputter grown interfaces show some ferromagnetism at lower temperature but the order of magnitude is the same as in the STO substrate. The effects of heating on STO substrate was studied by growing a 0 nm film (LA115). It is clear that growing a film on $TiO_2$-singly terminated STO (Figure 6.22 and Figure 6.23) or

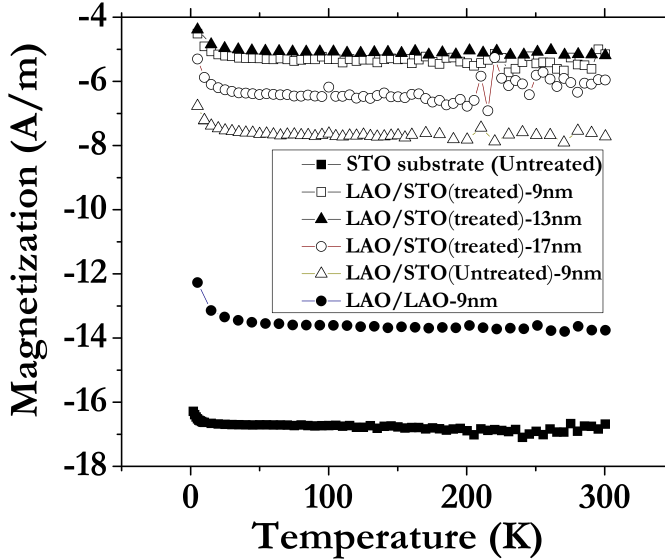


Figure 6.24: Temperature dependence of magnetization measured in 1 T for all films of LAO grown on untreated STO, treated STO and LAO substrates.

not growing at all (Figure 6.21) does not influence $M_s$ or the M-H loop. The sputter grown interfaces show ferromagnetic behavior which is not a pure or partly LAO/STO interface effect, nor that of LAO films. The thickness of the LAO film in this scenario is not relevant, although thicker films needs more heating time to grow, which may affect $M_s$. Note that $M_s$ increases when going from a 5 nm LAO film to 9 nm to 20 nm. It is also evident from the temperature dependent magnetization that treated STO is less diamagnetic than untreated STO. It seems that treated STO substrates may get some impurities during treatment or the annealing process itself reduces STO substrates to slightly ferromagnetic.

The measured ferromagnetism in the STO substrate is 5 times less than measured by Ariando *et al.* for LAO/STO PLD grown interfaces [30]. Taking a typical measured value of $5\times10^{-7}$ emu ($=5\times10^{-10}$ Am$^2$) for a 5 mm $\times$ 5 mm substrate, this would correspond to 0.3 $\mu_B$ for one surface unit cell of STO, or interface unit cell of LAO/STO. The same value is calculated by Liu *et al* for LAO/STO interface grown by PLD and measured by torque magnetometery [32]. It can be concluded, taking the 5 nm film as an example, that the interface magnetism in our sputter-grown LAO/STO films amounts to less than 0.15 $\mu_B$ per unit cell, and given the presence of ferromagnetism in the substrates probably even much less. This conclusion is qualitatively similar to the one reached in ref. [37], where no magnetism was found in STO/LAO multilayers.

### 6.6.5 Conclusion

We cannot exclude the possibility that our sputter grown interfaces are ferromagnetic, since the observations are hampered by the presence of ferromagnetism in the STO substrates. Still, since the numbers for the magnetic moments with and without the STO/LAO interface are similar, we conclude that the amount of magnetism is smaller than 0.15 $\mu_B$ per interface unit cell, and much smaller than reported in Refs. [30, 32].

# Bibliography

[1] O. Ohtomo, H. Hwang, Nature **427**, 423 (2004).

[2] D.G. Schlomm, and J. Mannhart, Nat. Mat. **10**, 68 (2011).

[3] M. Huijben, A. Brinkman, G. Koster, G. Rijnders, H. Hilgenkamp and D.H.A. Blank, Adv. Mat. **21**, 1665 (2009).

[4] G. Herranz, M. Basletic, M. Bibes, C. Carretero, E. Tafra, E. Jacquet, K. Bouzehouane, C. Deranlot, A. Hamzic, J. - M.Broto, A. Bathelemy, and A.Fert, Phys. Rev. Lett. **98**, 216803 (2007).

[5] W. Siemons, G. Koster, H. Yamamoto, W.A. Harrison, G. Lucovsky, T.H. Geballe, D.H.A. Blank and M.R. Beasley, Phys. Rev. Lett. **98**, 196802 (2007).

[6] A. Kalabukhov, R. Gunnarsson, J. Borjessen, E. Olsson, T. Claeson, D. Winkler, Phys. Rev. B **75**, 121404(R) (2007).

[7] C. Cancellieri, N. Reyren, S. Gariglio, A. D. Caviglia, and J.-M. Triscone, Euro, Phys. Lett. **91**, 17004 (2010).

[8] A. Kalabukhov, Y.A. Boikov, I.T. Serenkov, V.I. Sakharov, J. Borjesson, N. Ljustine, E. Olsson, D. Winkler and T. Claeson, Europhys. Lett. **93**, 37001 (2011).

[9] P.R. Willmott, S.A. Pauli, R. Herger, C.M. Schleputz, D. Martcoccia, B.D. Patterson, B. Delley, R. Clarke, D. Kumah, C. Cionca and Y. Yacoby. Phys. Rev. Lett. **99**, 155502 (2007).

[10] S.A. Chambers, M.H. Engelhard, V. Shutthanandan, Z. Zhu, T.C. Droubay, L. Qiao, P.V. Sushkob, T. Feng, H.D. Lee, T. Gustafsson, E. Garfunkel, A.B. Shah, J.-M. Zuo, Q.M. Ramasse, Surf. Sci. Rep. **65**, 317-352 (2010).

[11] M.P. Warusawithana, A.A. Pawlicki, T. Heeg, D.G. Schlom, C. Richter, S. Paetel, J. MANNHART, M. Zheng, B. Mulcahy, J.N. Eckstein, W. Zander, and J. Schubert, Bulletin of the APS **55**, nr. 2 (2010), abstract ID BAPS.2010.MAR.B37.1.

[12] B. Förg, C. Richter, ang J. Mannhart, Appl. Phys. Lett. **100**, 053506 (2012).

[13] L. Qiao, T.C. Droubay, T. Varga, M.E. Bowden, V. Shutthanandan, Z. Zhu, T.C. Kaspar, and S.A. Chambers, Phys. Rev. B **83**, 085408 (2011).

[14] C.W. Schneider, M. Esposito, I. Marozau, K. Conder, M. Doebeli, Ti Hu, M. Mallepell, A. Wokaun, and T. Lippert, Appl. Phys. Lett. **97**, 192107 (2010).

[15] S.A. Chambers, Surf. Sci. **605**, 1133 (2011).

[16] C.S. Hellberg, Bulletin of the APS **56**, nr. 1 (2011), abstract ID BAPS.2011.MAR.A34.5.

[17] S. Thiel, G. Hammert, A. Schmehl, C.W. Schneider, J. Mannhart, Science **313**, 1942 (2006).

[18] M. Huijben, G. Rijnders, D.H.A. Blank, S. Bals, S. Aert, J. Verbeeck, G. Tendeloo, A. Brinkman, and H. Hilgenkamp, Nature **5**, 556 (2006).

[19] M.L. Scullin, J. Ravichandran, C. Yu, M. Huijben, J. Seidel, A. Majumdar, R. Ramesh, Acta Mater. **58**, 457 (2010).

[20] A. Brinkman, M. Huijben, M. van Zalk, J. Huijben, U. Zeitler, J.C. Maan, W.G. van der Wiel, G. Rijnders, D.H.A. Blank, and H. Hilgenkamp, Nature Materials **6**, 493 (2007).

[21] N. Nakagawa, H.Y. Hwang and D.A. Muller, Nature Materials **5**, 204 (2006).

[22] N. Reyren, S. Thiel, A.D. Caviglia, L.F. Kourkoutis, G. Hammerl, C. Richter, C.W. Schneider, T.H-. Kopp, A.-S. Ruetschi, D. Jaccard, M. Gabay, D.A. Muller, J.-M Triscone, J. Mannhart, Science **317**, 1196 (2007).

[23] A.D. Caviglia, S. Gariglio, N. Reyren, D. Jaccard, T. Schneider, M. Gabay, S. Thiel, G. Hammerl, J. Mannhart, and J.-M. Triscone, Nature **456**, 624 (2008).

[24] Y.Z. Chen, D.V. Christensen, F. Trier, N. Pryds, A. Smith, S. Linderoth, Appl. Surf. Science **258**, 9242 (2012).

[25] C. Bell, S. Harashima, Y. Hikita, and H.Y. Hwang, Appl. Phys. Lett. **94**, 222111 (2009).

[26] C.W. Bark, D.A. Felker, Y. Wnag, Y. Zhang, H.W. Jang, C.M. Folkman, J.W. Park, S.H. Baek, H. Zhou, D.D. Fong, X.Q. Pan, E.Y. Tsymbal, M.S. Rzchowski, and C.M. Eom, PNAS **108**, 4720, (2011).

[27] R. Pentcheva, and W.E. Pickett, Phys. Rev. B **74**, 035112 (2006).

[28] P. Delugas, Phys. Rev. Lett. **106**, 166807 (2011).

[29] Z.S. Popovic, S. Satpathy, and R.M. Martin, Phys. Rev. Lett. **101**, 256801 (2008).

[30] Ariando, X. Wang, G. Baskaran, Z.Q. Liu, J. Huijben, J.B. Yi, A. Annadi, A.R. Barman, A. Rusydi, S. Dhar, Y.P. Feng, J. Ding, H. Hilgenkamp, T. Venkatesan, Nat. Comm. **2**, 188 (2011).

[31] J.A. Bert, B. Kalisky, C. Bell, M. Kim, Y. Hikita, H.Y. Hwang, and K.A. Moler. Nature Phys. **7**, 767 (2011).

[32] L. Li, C. Richter, J. Mannhart, R.C. Ashoori, Nature Phys. **7**, 762766 (2011).

[33] B. Kalisky, J.A. Bert, B.B. Klopfer, C. Bell, H.K. Sato, M. Hosoda, Y. Hikita, H.Y. Hwang, K.A. Moler, Nature Commu. **3**, 922 (2012).

[34] N. Pavlenko, T. Kopp, E.Y. Tsymbal, G.A. Sawatzky, J. Mannhart, arXiv:1105.1163 (2011)

[35] K. Michaeli, A.C. Potter, and P.A. Lee [arXiv:1107.4352 (2011).

[36] H.P.R. Frederikse, and G.A. Candela, Phys. Rev. **147**, 583 (1966).

[37] M.R. Fitzsimmons, N.W. Hengartner, S. Singh, M. Zhernenkov, F.Y. Bruno, J. Santamaria, A. Brinkman, M. Huijben, H.J.A. Molegraaf, J. de la Venta, and I.K. Schuller, Phys. Rev. Lett. **107**, 217201 (2011).